



Influence of the Heat Transfer Field on Anomalous Lubricant Film Formation in Elastohydrodynamic Lubrication Conditions

Kazuyuki Yagi¹ · Kazuki Nishida² · Joichi Sugimura¹

Received: 6 May 2021 / Accepted: 26 July 2021 / Published online: 7 August 2021
© The Author(s), under exclusive licence to Springer Science+Business Media, LLC, part of Springer Nature 2021

Abstract

The influence of the heat transfer field on anomalous film formation under elastohydrodynamic lubrication (EHL) conditions was studied. Liquid lubricant film shapes between a transparent disc and steel ball friction pair were investigated by white light optical interferometry. The fatty alcohol 1-dodecanol was used as the representative lubricant to develop anomalous film shapes. A sapphire disc and glass disc, which have different thermal conductivities, were used as the transparent bounding surface. Experiments were performed wherein the applied load, sliding conditions and ambient temperature were varied. The temperature of the lubricant film was estimated by a simple model with the measured traction coefficient. The estimated temperature and maximum Hertzian pressure were compared with the phase diagram of 1-dodecanol obtained using a diamond anvil cell to investigate the phase state of the lubricant film. It was found that the anomalous film shape was stably formed in the solid-state regime of the phase diagram whereas the film exhibited unique characteristics such as the collapse behaviour in high sliding conditions and liquid-like behaviour of the traction with a remaining thickened film part in the liquid state regime.

Keywords Elastohydrodynamic · Film shape · Rheology · Phase transition · Solidification · Temperature

1 Introduction

Elastohydrodynamic lubrication (EHL) has been one of the most important topics in the tribological field for over a century. Pressure develops at the entrance of the contact area and builds up to the order of several gigapascals. A significantly high pressure causes large elastic deformations of the bounding surfaces and an increase in the viscosity of the lubricant, termed as the piezoviscous effect [1]. The film formed in the lubricated area has a specific shape with a flat part around the contact area and a constricted shape at the exit zone [2]. A lubricant film with a thickness of less than

1 μm is greatly sheared under the movement of the bounding surfaces at speeds of several metres per second.

For a better understanding of EHL, both the traction and the film thickness are important information. Traction is generated in the contact area, where a lubricant film of significantly high viscosity is sheared at a high shear rate of the order of 10^6 s^{-1} . A lubricant film under significant shearing force does not exhibit the Newtonian rheological behaviour. Instead, it shows shear thinning, viscoelastic, or elastoplastic behaviour [3–8]. On the contrary, it has been recognised that the film thickness is determined by the flow at the entrance with a great geometrical convergent shape [9]. The formed film has a specific shape; it is flat around the central area and constricted at the exit zone [2]. Representative formulas have been suggested for the film thickness at the centre and minimum film thickness for conveniently designing the lubricated area [10]. A fast numerical simulation algorithm has also been developed for solving the EHL problems [11].

Further, the influence of the rheological characteristics of the lubricant within the lubricated area on the film formation has attracted increasing interest over the last two decades. Significant variations in the film shape were identified under rolling/sliding conditions [12–20] and opposite sliding

✉ Kazuyuki Yagi
yagik@mech.kyushu-u.ac.jp

¹ Department of Mechanical Engineering, Faculty of Engineering, International Institute for Carbon-Neutral Energy Research (I²CNER), Kyushu University, 744 Motoooka, Nishi-ku, Fukuoka 819-0395, Japan

² Department of Hydrogen Energy Systems, Graduate School of Engineering, Kyushu University, 744 Motoooka, Nishi-ku, Fukuoka 819-0395, Japan

conditions at a zero entrainment speed [21, 22], and in the cases of high-viscosity oil [23] and liquids with a clear melting point [24–30]. Variations in the film shape under rolling/sliding conditions [12–20] and opposite sliding conditions [21, 22] were concluded to arise from the viscosity wedge action [31], whereas the film shape variations in the cases of high-viscosity oils [23] and liquids with a clear melting point [24–30] remain to be fully understood.

Herein, we present the appearance of anomalous film shapes in the case of a liquid with a clear melting point [24–30]. Anomalous film shapes were discovered at the point contact area between a glass disc and a steel ball lubricated with a fatty alcohol, 1-dodecanol [24–27]. Under pure rolling conditions, the film was found to have the conventional shape [2]. The shape of the film however changed, resulting in a gradual increase in the film thickness around the central zone with increasing slide-to-roll ratio. At high slide-to-roll ratios, the thickened part moved towards the entrance, and then a thinner part of the film dominated. The film shape depended on the sign of the slide-to-roll ratio at high slide-to-roll ratios; the thickened part tended to move towards the entrance at higher steel ball speeds, whereas it tended to remain in the lubricated area at higher glass disc speed. In ensuing studies, other fatty alcohols [26], an acid, an amine, a chloride, and various alkanes [28] were found to adopt the same film shape as 1-dodecanol. Furthermore, the maximum traction coefficient was observed at a low slide-to-roll ratio, and the value decreased gradually with increasing slide-to-roll ratio for 1-dodecanol and other liquids that developed anomalous film shapes. In contrast, liquids developing the conventional film shape exhibited a gradual increase in the traction coefficient with increasing slide-to-roll ratio [28]. The shear rate of the maximum traction coefficient for liquids developing anomalous film shapes ranged from 10^5 to 10^7 s^{-1} , which is of the same order as those of traction fluids [29]. The shear rate depends on the liquid type; for example, the shear rates for *n*-tetradecane and *n*-hexadecane (alkanes) are $\sim 2.0 \times 10^6$ s^{-1} , whilst that of 1-dodecanol (an alcohol) is $\sim 4.0 \times 10^5$ s^{-1} . Reddyhoff et al. [30] focused on the transition of the traction behaviour of 1-dodecanol with pressure and ambient temperature.

The anomalous film formation in the case of liquids with a clear melting point [24–30] has been attributed to the solidification of the lubricant. In a previous study [25], a small temperature rise of ~ 30 °C was estimated using a simple temperature formula based on the assumption of semi-infinite bodies. However, the heat generated in the film influences the formation of anomalous film shapes, because the possibility can be predicted based on the trend of the traction coefficient with increasing slide-to-roll ratio and a significant difference in the film shapes at positive and negative slide-to-roll ratios at the glass–steel contact. Therefore, in the current study, we focused on the influence

of the heat transfer field on the film formation. White light optical interferograms of the film formed at the point contact area between a transparent disc (glass or sapphire) and steel ball were captured. Sapphire and glass with different thermal conductivities were used as one of the surface materials to change the heat transfer field of the friction surfaces. The formation of the anomalous film shapes was investigated by changing the material of one of the bounding surfaces, sliding conditions, and ambient temperature.

2 Experimental Procedure

Tests were conducted using a ball-on-disc type test rig, as reported previously [28, 29], to study the variations in the lubricant film thickness and traction. Figure 1 shows a schematic of the test rig. A point contact area was created between a rotating transparent disc (diameter: 80 mm; thickness: 5 mm) and a rotating steel ball (diameter: 25.4 mm). SUJ2, which is equivalent to AISI52100, was used as the steel substrate. The rotational speeds of the disc and ball are independently controlled using AC servo motors to set desired slide-to-roll ratios. The ball and disc are placed in a chamber containing the lubricant. The temperature of the chamber is controlled using a heating system consisting of heat pipes, a thermistor, and a controller. The lubricant is supplied to the contact area by ball rotation. An optical microscope is installed above the test rig to measure the film thickness via white light optical interferometry. White light from the microscope is illuminated onto the contact area, and the reflected light is captured by a digital camera attached to the microscope. A thin chromium layer was deposited on the contact side of the disc surface to increase the contrast of the optical interferograms between the transparent disc surface and steel ball.

A BK7 glass disc or a sapphire disc was used as the transparent material. Both these materials are transparent to visible light, but have different thermal conductivities. Table 1 lists the bulk properties of the materials of the two discs and steel ball counterpart. A fatty alcohol, 1-dodecanol, was used as the representative liquid lubricant that develops anomalous film shapes, as demonstrated in previous studies [24–28].

The slide-to-roll ratio, S is defined as follows:

$$S = \frac{u_b - u_d}{u_m} \quad (1)$$

where u_b is the ball speed and u_d is the disc speed. The entrainment speed, u_m is defined as $u_m = (u_b + u_d)/2$. When the ball speed is higher than the disc speed, S is positive, and when the ball speed is lower than the disc speed, S is negative. All tests were conducted at a constant u_m of 1.8 m/s.

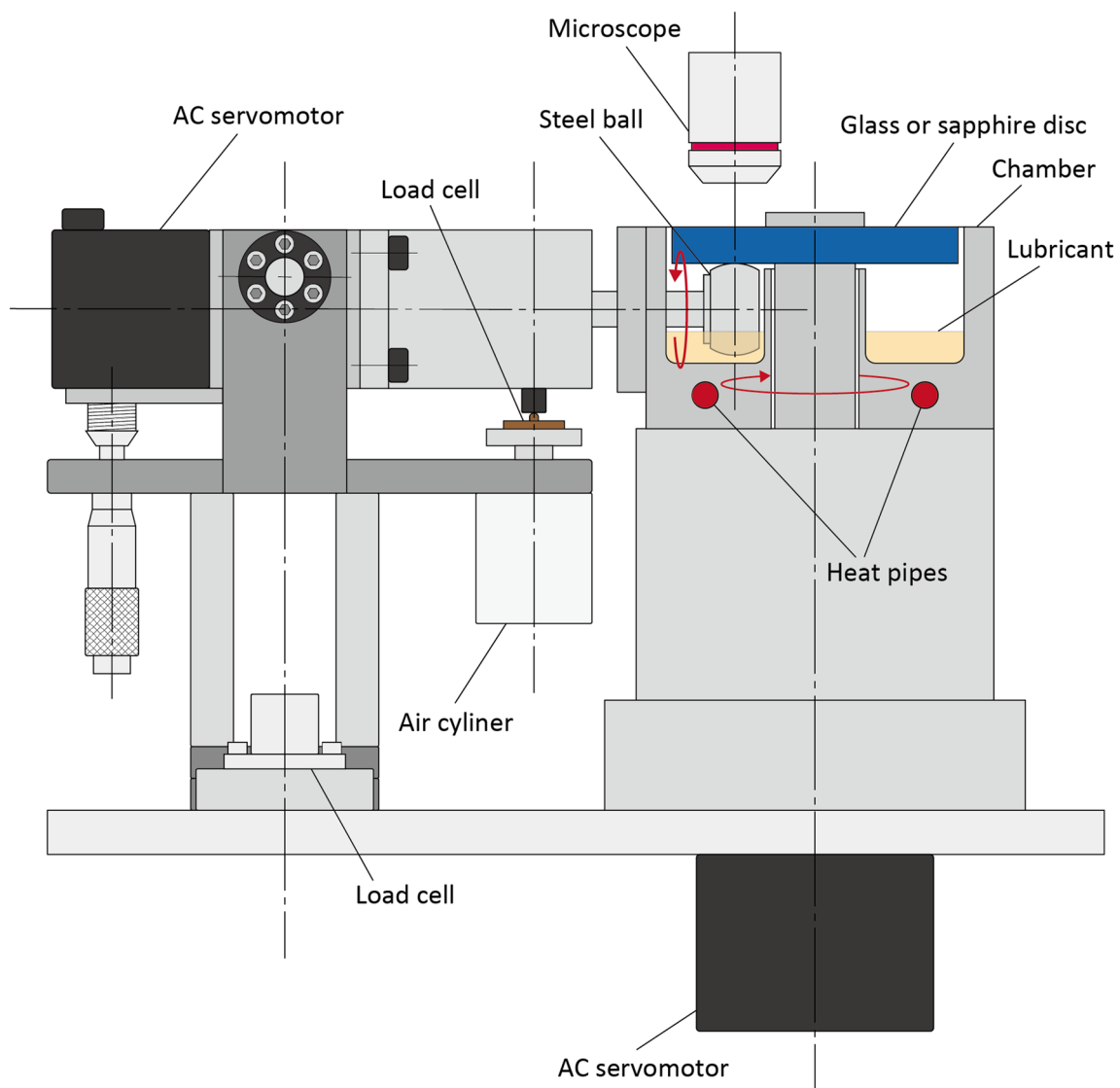


Fig. 1 Schematic of the test rig

Table 1 Bulk properties of steel, glass, and sapphire

Properties	Steel	Glass	Sapphire
Young's modulus (GPa)	210	81	365
Poisson's ratio	0.300	0.208	0.2
Density (kg/m^3)	7850	2510	3980
Thermal conductivity (W/mK)	46.00	1.11	27.00
Specific heat (J/kg K)	470	840	577

The phase diagram of 1-dodecanol was constructed using a diamond anvil cell device. Figure 2 shows a schematic of the diamond anvil cell device. A gasket of stainless steel SUS304 (thickness: 0.5 mm) with a 0.6 mm diameter hole was sandwiched between the diamond anvils

with a currette diameter of 1.2 mm. A small amount of the lubricant, 1-dodecanol, and a piece of ruby were introduced into the hole. A hydraulic pressure was applied to the lubricant by tightening a screw attached to the device. The temperature of the device was controlled using a heating system consisting of heat pipes, a K-type thermocouple, and a controller. The pressure was calculated on the basis of the fluorescence of ruby [32]. The phase state of the lubricant was observed with a transmission optical microscope. The phase state of the lubricant was confirmed from the appearance of the lubricant crystal grains in the visible images with increasing pressure at a constant temperature.

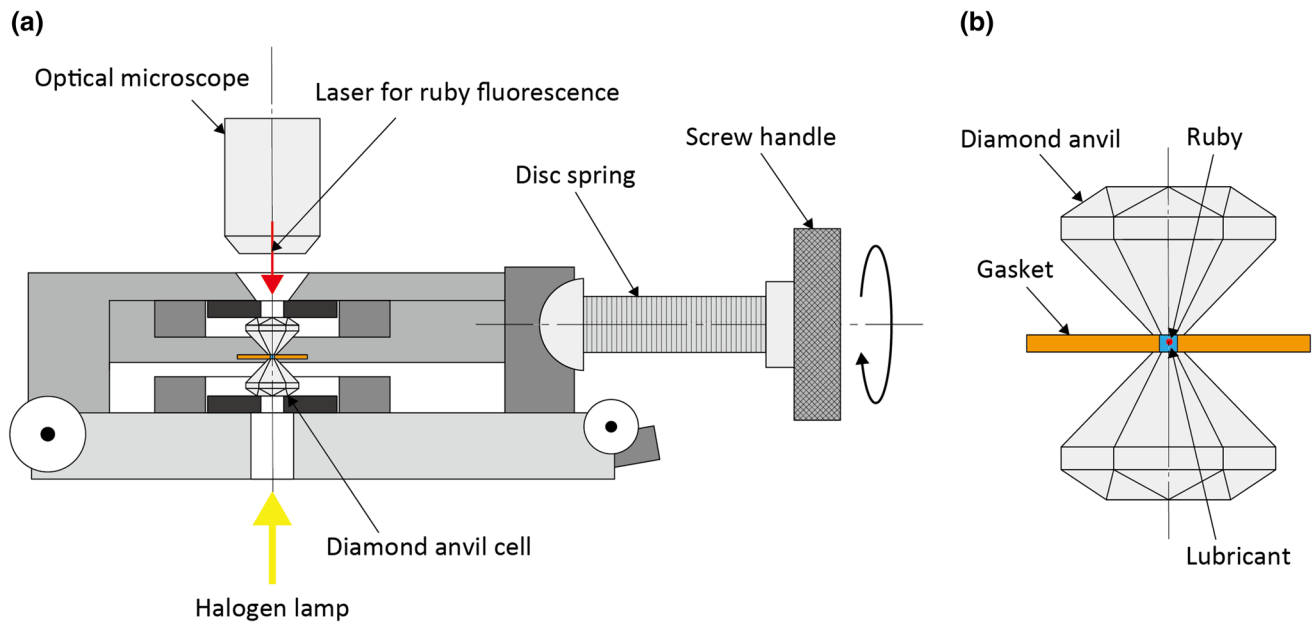


Fig. 2 Schematic of the diamond anvil cell device. **a** Full view of the device and **b** enlarged view of the diamond anvil cell

3 Results

Figure 3 shows the optical interferograms of the 1-dodecanol film at the glass–steel contact under different slide-to-roll ratios. The operating conditions are the same as those used in previous studies [28, 29]. They allowed us to follow the trend of the film thickness in detail. Under pure rolling conditions, the film had a conventional shape with a flat part in the central zone and a constricted part at the exit zone. The film thickness changed with increasing slide-to-roll ratio. At $S < 0.9$, the shapes of the lubricant

film were similar at the same absolute value of S . At $S > 1.2$, the film collapsed around the central zone with an increasing S when S is positive, whereas it was thick when S is negative. Figure 4 shows the optical interferograms of the film at the sapphire–steel contact under different slide-to-roll ratios. The general trend of the variation in the film thickness was the same as that of the glass–steel contact. Three main differences were observed in the film formation between the glass–steel and sapphire–steel contact pairs. The first is the size of the contact area; the contact area at the sapphire–steel contact was smaller than that at the glass–steel contact because of the higher elasticity

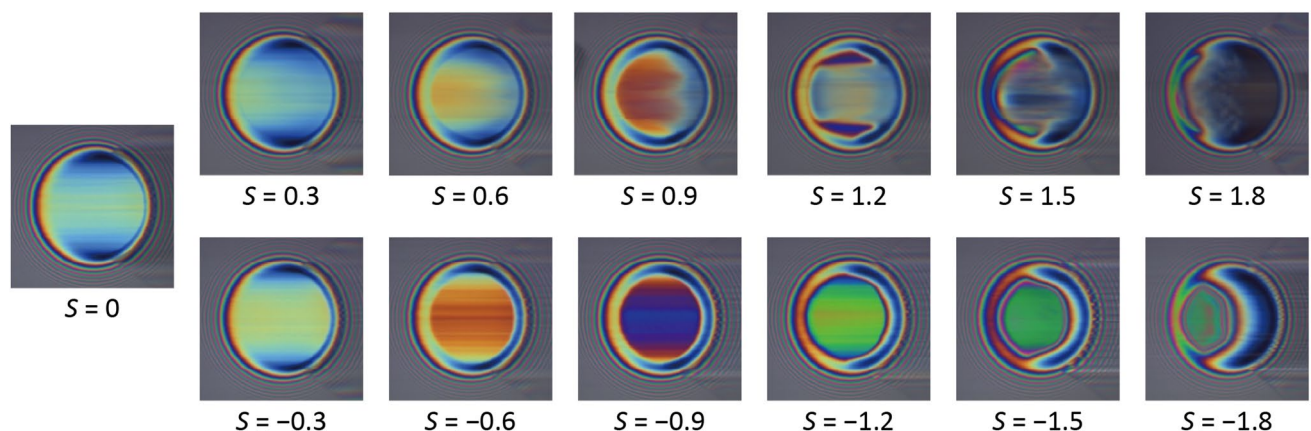


Fig. 3 Optical interferograms of the lubricant film at the glass–steel contact at different slide-to-roll ratios under the applied load W of 40 N (the maximum Hertzian pressure and Hertzian radius were 0.57 GPa and 183 μm , respectively) and ambient temperature T_0 of 30 $^{\circ}\text{C}$

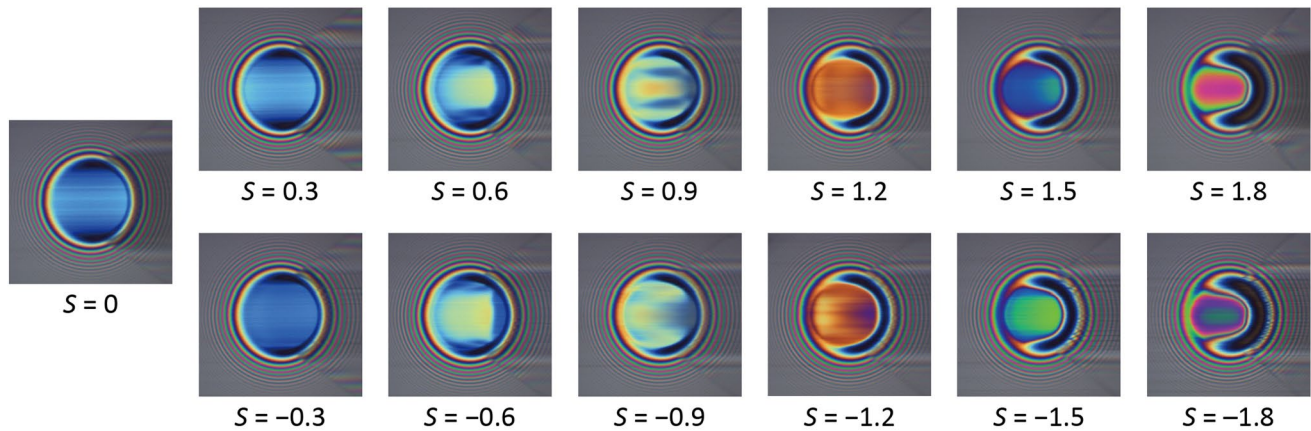


Fig. 4 Optical interferograms of the film at the sapphire–steel contact at different slide-to-roll ratios under the applied load W of 40 N (the maximum Hertzian pressure and Hertzian radius were 1.00 GPa and 138 μm , respectively) and ambient temperature T_0 of 30 $^{\circ}\text{C}$

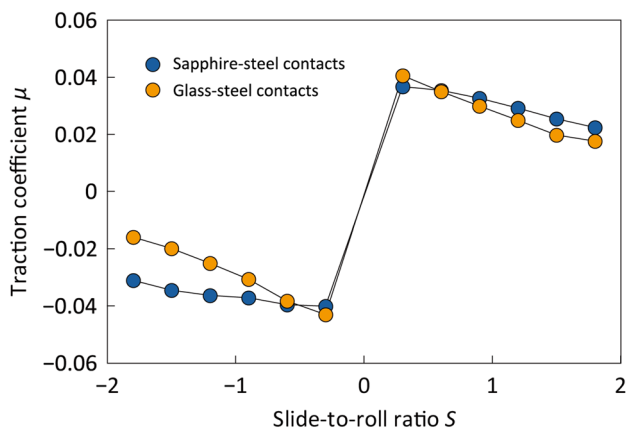


Fig. 5 Variations in the traction coefficient with the slide-to-roll ratio S under the applied load W of 40 N and ambient temperature T_0 of 30 $^{\circ}\text{C}$

of sapphire than that of glass, as shown in Table 1. The second difference is the film thickness; the film was thinner at the sapphire–steel contact than at the glass–steel contact. The third difference is the symmetry of the film formed at positive and negative S values; the film thickness was not symmetrical with respect to S at the glass–steel contact, whereas the film developed the same shape at the sapphire–steel contact, regardless of the sign of S (i.e., at positive S and negative S).

Figure 5 shows the variation in the traction coefficient with the slide-to-roll ratio. The traction coefficient had the maximum value at low S , and then it decreased monotonically with increasing S . The maximum values of the traction coefficient at the sapphire–steel contact were smaller than those at the glass–steel contact. However, the traction coefficient at the sapphire–steel contact was greater than that at the glass–steel contacts at greater S , because of the

marginal decrease in the traction coefficient with S at the sapphire–steel contact.

Figure 6 shows the optical interferograms recorded to study the film thickness variation at the glass–steel contact at the ambient temperatures T_0 of 30, 50, and 70 $^{\circ}\text{C}$ under different positive S values, whilst Fig. 7 shows the variation under the same conditions under negative S values. Figure 8 shows the variation in the traction coefficient under the same operating conditions as those of Fig. 6 (i.e., at different positive S values). The tests were conducted to investigate the film formation and traction behaviours of 1-dodecanol when the phase state changed from liquid to solid in the lubricated area. The phase state of 1-dodecanol was confirmed from the maximum Hertzian pressure, ambient temperature, and its phase diagram shown later. Both the film thickness and the shape changed with increasing ambient temperature T_0 . Under pure rolling conditions, the film thickness decreased to less than 70 nm at 70 $^{\circ}\text{C}$ because of the decrease in the viscosity of 1-dodecanol. However, the thicker part of the film around the central zone remained even at the ambient temperature T_0 of 70 $^{\circ}\text{C}$, when 1-dodecanol appeared to be in the liquid state. The thickened part of the film showed a greater tendency to remain at a higher negative S than at positive S at the ambient temperature T_0 of 30 $^{\circ}\text{C}$, whereas the trend was reversed at the ambient temperature T_0 of 70 $^{\circ}\text{C}$. The traction coefficient decreased with increasing ambient temperature T_0 . The trend of the traction coefficient with respect to S at 70 $^{\circ}\text{C}$ was different from the trends at 30 and 50 $^{\circ}\text{C}$; the traction coefficient increased gradually with increasing S at 70 $^{\circ}\text{C}$.

Figure 9 shows the variation in the optical interferograms with a change in the ambient temperature T_0 at a constant S of 0.6 and constant maximum Hertzian pressure of 0.36 GPa, which is the minimum value that could be applied with the test rig used in this study. The film thickness decreased

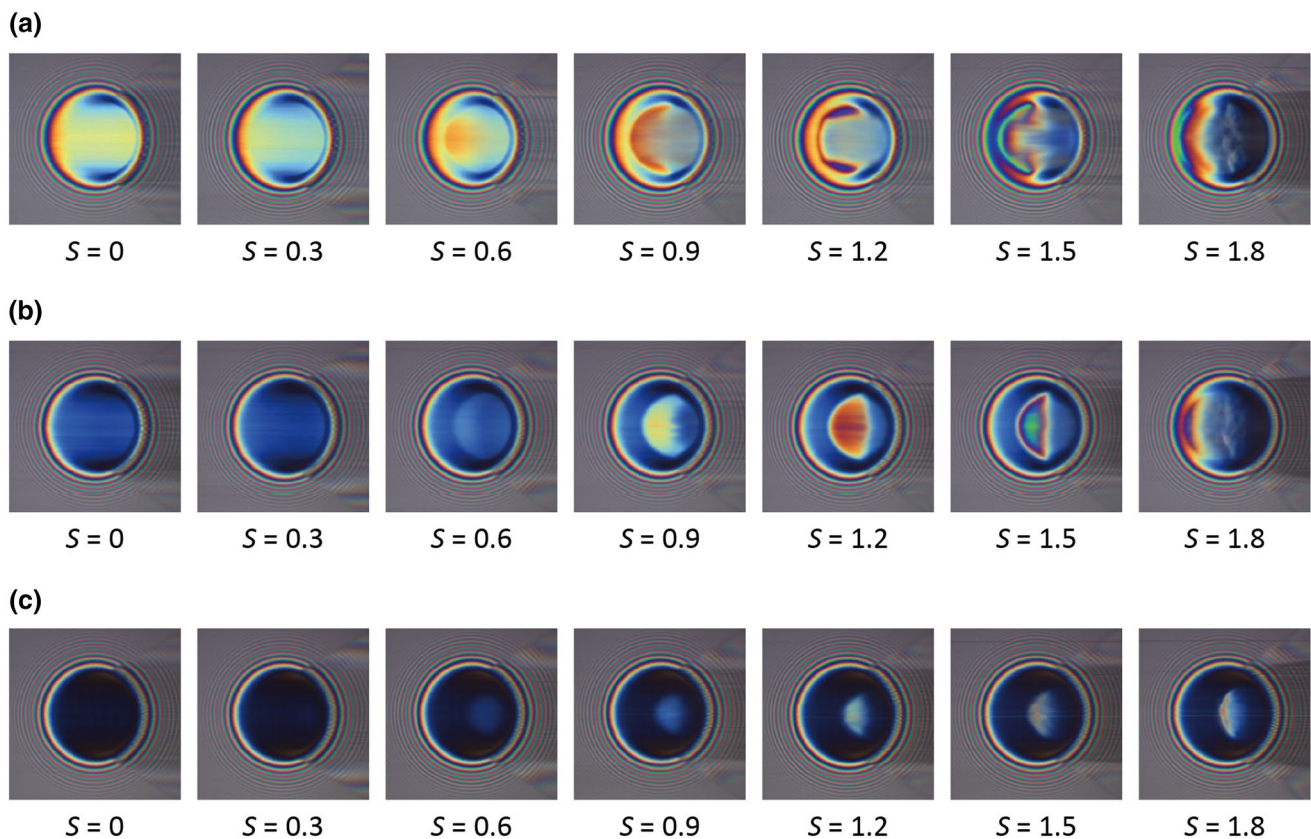


Fig. 6 Variations in the optical interferograms of the film at the glass–steel contact under the applied load W of 20 N (the maximum Hertzian pressure was 0.45 GPa) at different positive slide-to-roll ratios S and ambient temperatures T_0 of **a** 30, **b** 50, and **c** 70 °C

with increasing ambient temperature T_0 , but the thickened part remained around the central zone.

4 Discussion

The tests revealed that the anomalous film shape and traction coefficient of 1-dodecanol depend on the heat transfer conditions, such as the material of the bounding surfaces and ambient temperature. At the glass–steel contact, the shape/thickness of the film and traction coefficient depend on the sign of S at the ambient temperature T_0 of 30 °C; a thin film part expanded over the lubricated area at a high positive S value with a higher ball speed, whereas a thick part of the film remained at a high negative S value with a lower ball speed, as shown in Fig. 3. The traction coefficient at the glass–steel contact was not symmetrical to the sign of S ; it decreased at a higher rate with an increasing sliding speed at a negative S . The asymmetry of the film shape to the sign of S disappears with an increasing ambient temperature T_0 , as shown in Figs. 6 and 7. In contrast, at the sapphire–steel contact, the shape/thickness of the film and traction coefficient were almost symmetrical with respect to the sign of

S ; a thick film existed between the inlet zone and central zone, and the film was slightly thinner at positive S than at negative S , as shown in Fig. 4.

These differences in the film formation and traction behaviours can be attributed to the different thermal conductivities of the glass and sapphire discs. The thermal conductivity of glass is significantly lower than that of sapphire (Table 1). It is well-recognised that the thermal properties of bounding surfaces greatly influence the film formation characteristics. One of the representative findings on the influence of the thermal properties of the bounding surfaces is a dimple discovered by Kaneta et al. [19, 20], which appeared under simple sliding contact conditions between a moving glass disc and stationary steel ball counterpart, but was not observed when the steel surface was slid against the stationary glass disc. The thick film formation in the current study is the opposite trend to the dimpling phenomenon reported by Kaneta et al. [19, 20]. The thermal conductivity of sapphire is closer to that of steel but differs from that of glass as shown in Table 1. However, Reddyhoff et al. [33] reported that the thermal conductivity of steel within a depth of $\sim 10 \mu\text{m}$ was 21 W/mK, which is lower than the value of 46 W/mK cited in previous studies. Other studies [34, 35]

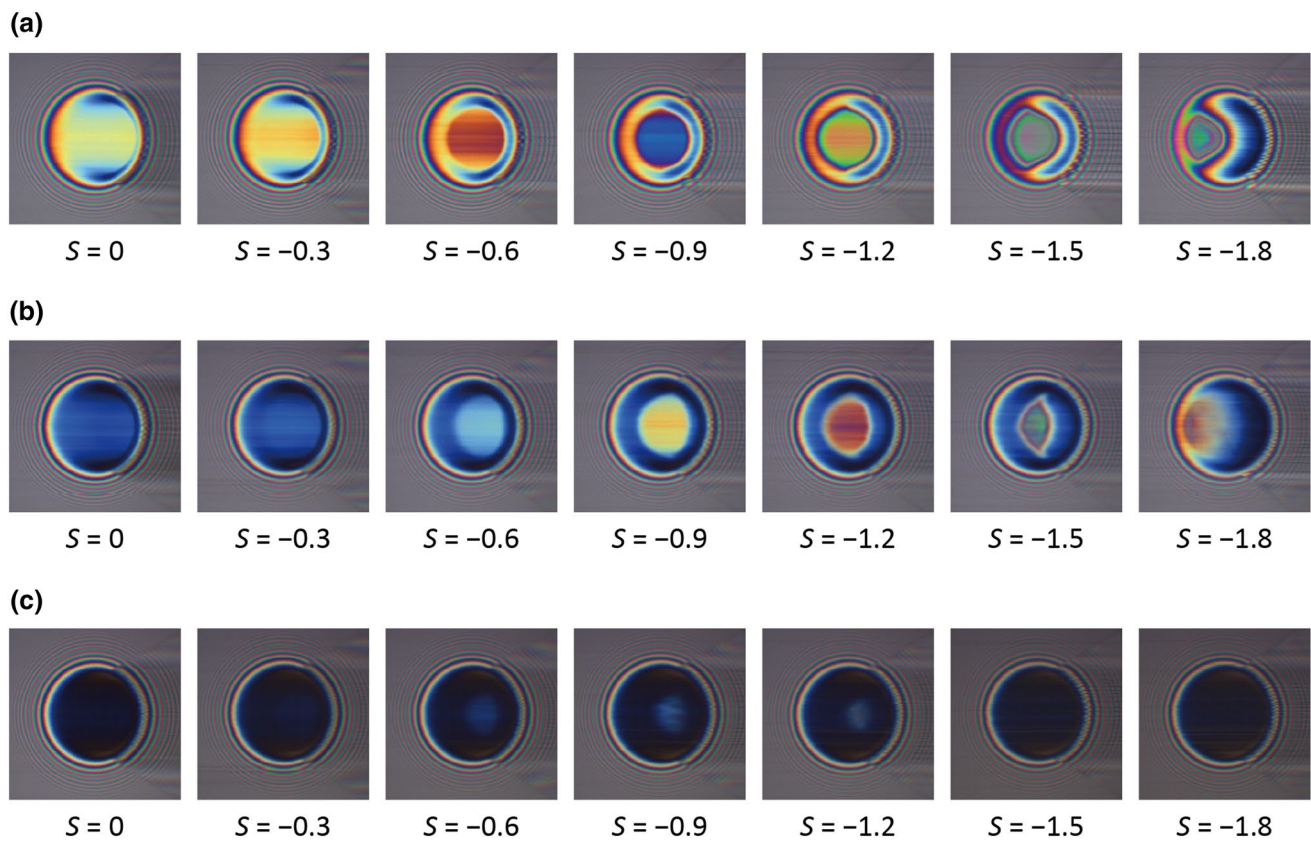


Fig. 7 Variations in the optical interferograms of the film thickness at the glass–steel contact under the applied load W of 20 N (the maximum Hertzian pressure was 0.45 GPa) at different negative slide-to-roll ratios S and ambient temperatures T_0 of **a** 30, **b** 50, and **c** 70 °C

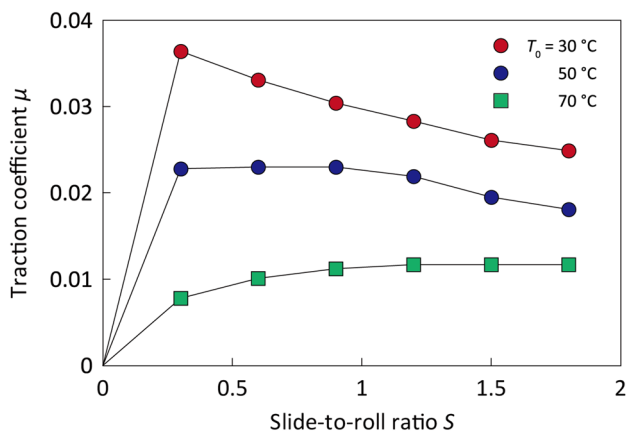


Fig. 8 Variations in the traction coefficient at the glass–steel contact under the applied load W of 20 N (the maximum Hertzian pressure was 0.45 GPa) at different slide-to-roll ratios S and different ambient temperatures T_0 of 30, 50, and 70 °C. The operating conditions were the same as those of Fig. 6

discussed the impact of the thermal properties on the traction behaviour. The thermal conductivity of 21 W/mK measured by Reddyhoff et al. [33] is close to that of sapphire. The

symmetrical behaviours of the film and traction can probably be attributed to the comparable thermal conductivities between the surfaces.

A solid-like behaviour was indicated by the variations in the traction coefficient as well as the film thickness/shape. The maximum traction coefficient at a low S , and a gradual decrease in the traction coefficient with increasing S were observed, as shown in Fig. 5. This is a typical trend observed in the cases of traction oils [6–8], which were speculated to behave like elastoplastic materials. Further, a decrease in the traction coefficient with increasing ambient temperature T_0 , which is shown in Fig. 8, has also been observed for traction fluids [6–8]. Notably, in Fig. 8, the gradual increase in the traction coefficient with S at the ambient temperature T_0 of 70 °C is different from the trend observed at the other lower ambient temperatures. The trend observed at 70 °C is similar to the trends of ethylene glycol and glycerol, which develop conventional film shapes [28, 29]. However, a thickened part of the film appeared around the central zone at the ambient temperature T_0 of 70 °C, as shown in Figs. 6 and 9.

Figure 10 shows the phase diagram of 1-dodecanol obtained using a diamond anvil cell. A change in the solid state was confirmed from the appearance of crystal grains

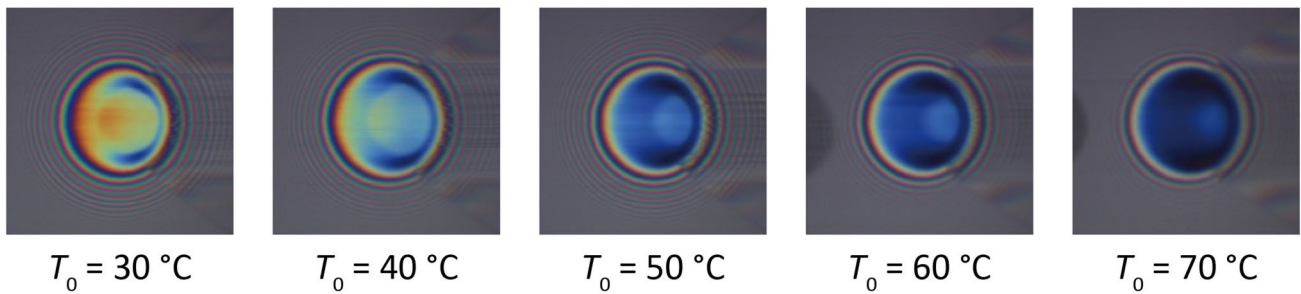


Fig. 9 Variations in the optical interferograms of the film thickness at the glass–steel contact under the applied load W of 10 N (the maximum Hertzian pressure was 0.36 GPa) and constant slide-to-roll ratio S of 0.6 at different ambient temperatures T_0

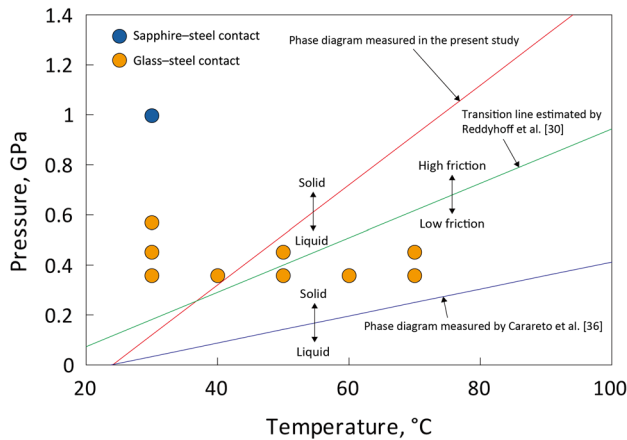
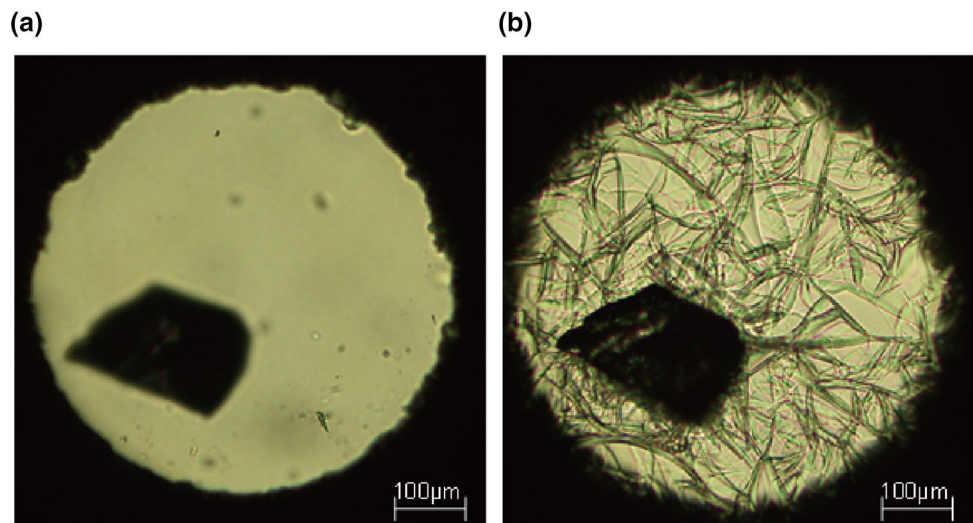


Fig. 10 Phase states of the lubricated area, as estimated from the ambient temperature and maximum Hertzian pressure

with increasing pressure. Figure 11 shows the visible images of 1-dodecanol in the liquid state at the atmospheric pressure and an appearance of crystal grains at a pressure of 30 MPa

and the temperature of 30 °C. The phase states at the contact area, which were estimated from the ambient temperature and maximum Hertzian pressure under the current operating conditions, are plotted in Fig. 10. The transition line between high friction and low friction estimated by Reddyhoff et al. [30] and the phase diagram obtained by Carareto et al. [36] are also depicted in Fig. 10. The phase diagram obtained in this study is remarkably different from that obtained by Carareto et al. [40]. This difference can be attributed to the difference in the measuring procedure of the melting point. Carareto et al. [36] measured the melting point based on the observation of the disappearance of crystal grains of solidified 1-dodecanol with decreasing pressure; in contrast, in this study, the appearance of crystal grains with increasing pressure formed the basis to determine the melting point at different temperatures. The lubricant film of 1-dodecanol formed anomalous shapes under all the operating conditions in this study. Thus, the phase diagram obtained by Carareto et al. [40] may be more reasonable. However, liquid-like trends were observed in the solid regime of the phase diagram measured by Carareto et al. [40], such as the traction

Fig. 11 Visible images of 1-dodecanol pressurised by the diamond anvil cell at **a** the atmospheric pressure and **b** at 60 MPa under a constant temperature of 30 °C



behaviour at the temperature of 70 °C (Fig. 8), and disappearance of the anomalous film shape at 70 °C and a high S (Fig. 7 (c)). Furthermore, the collapse of the film formation observed at a high S (Figs. 3, 6 and 7), which was also observed in past studies [25], likely indicate a phase state different from the solid phase state of the phase diagram.

Further investigation of the phase state of the lubricant film was conducted considering the heat generation in the film. The temperature of the lubricant film was also calculated using a simple model based on the assumption of semi-infinite bodies for bounding surfaces derived by Yagi et al. [25].

$$t_f = \frac{\mu p_{hm} \Delta u h}{12 k_f} + \frac{t_b + t_d}{2}, \tag{2}$$

$$t_b = \frac{1.464 q_b a}{k_b \sqrt{\pi (0.874 + Pe_b)}} \tag{3}$$

$$t_d = \frac{1.464 q_d a}{k_d \sqrt{\pi (0.874 + Pe_d)}} \tag{4}$$

$$Pe_b = \frac{u_b a}{2 \kappa_b}, Pe_d = \frac{u_d a}{2 \kappa_d}, \tag{5}$$

$$q_b = \frac{\mu p_{hm} \Delta u}{2} + k_f \frac{t_d - t_b}{h} \tag{6}$$

$$q_d = \frac{\mu p_{hm} \Delta u}{2} - k_f \frac{t_d - t_b}{h} \tag{7}$$

where t is the average temperature in the lubricated area, Pe is the Peclet number, q is the average heat flux flowing into the surface, a is the Hertzian radius, μ is the traction coefficient, Δu is the sliding speed, k is the thermal conductivity, κ is the thermal diffusivity, and subscripts of b, d and f denote the ball, disc and lubricant film, respectively. The derivation process of the equation is described in a previous paper [25]. For calculation of the temperature, the measured traction coefficients and central film thickness were incorporated into the equations.

Figure 12 shows the estimated temperatures at different S for the glass–steel contact shown in Fig. 3 and the sapphire–steel contact shown in Fig. 4. The temperature was calculated for two thermal conductivities of bulk steel and that of the top surface measured by Reddyhoff et al. [33]. It was found that there is a difference in the film formation at positive S values with respect to the melting point measured in this study. The temperature increased beyond the melting point with an increasing S for the glass–steel contact with the collapse of the film at positive S values, whereas the temperature was lower than the melting point, expect for $S = -1.5$ and -1.8 , for the sapphire–steel contact accompanied by the stable formation of the film. For positive S values, the steel surface with a higher moving speed exhibited a lower temperature than the counter surface with a slower moving speed [18, 25]. The temperature difference between both the mating surfaces probably influences the yield phenomenon of the film above the melting point. Therefore, the melting point measured in this study indicates a change in the phase state.

Regarding the solid-like behaviour of the film for the glass–steel contact even in the liquid state of the phase diagrams obtained in this study, there are three possibilities for the increase in the melting temperature of 1-dodecanol in

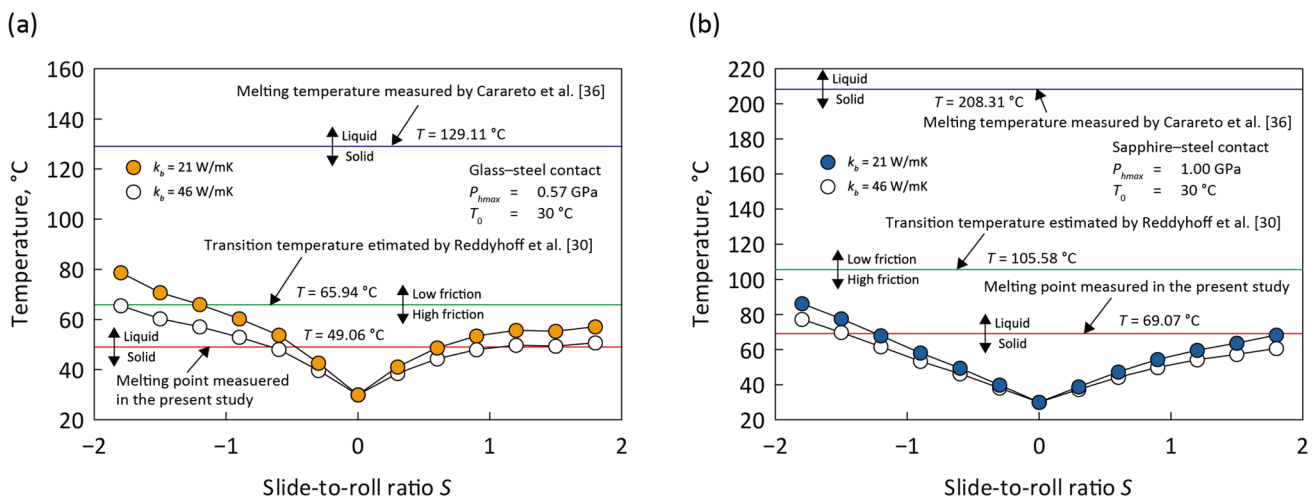


Fig. 12 Estimated temperature of the film at different slide-to-roll ratios for a the glass–steel contact and b the sapphire–steel contact

the lubricated area. The first is the alignment of the lubricant molecules along the sliding direction under high shear rates [37–39]. 1-dodecanol has a simple linear chain structure, and thus tends to align along the sliding direction. The second possibility is the increase in the melting point of a thin film confined between two solid surfaces. It has been reported that the melting point of a film on a solid surface increases for a monolayer of 1-dodecanol [40–45]. This might be a possibility, although the film is considerably thicker in the current study. The third possibility is the appearance of an α phase of metastable solid state with a rapid increase in the pressure whilst passing through the lubricated area, as reported by Reddyhoff et al. [30]. These three phenomena suppress the movement of the lubricant molecules; these are related to the adsorption of additives on surfaces as well as the solidification phenomenon described in the current study.

The current parametric study under varying slide-to-roll ratio, surface material, and ambient temperature in comparison with the phase diagram revealed the solid-like behaviour of the film formation and traction. Additionally, the current study provides key guidelines for further studies on the phase state of the lubricant film. Further studies on the mechanisms of the anomalous film formation can aid understand the other aspects of boundary lubrication as well as EHL and hydrodynamic lubrication.

5 Conclusions

In this study, the film formation behaviours and anomalous film shapes of a long-chain alcohol, 1-dodecanol, were investigated with a changing heat transfer field. Parametric experiments were conducted with a focus on the influence of the heat transfer conditions. BK7 glass and sapphire, which have significantly different thermal conductivities, were tested as one of the contact pairs. Optical interferograms of the film thickness were captured by changing the slide-to-roll ratio and ambient temperature. A phase diagram of 1-dodecanol was used to determine the phase state of the lubricant in the contact area. The following results were obtained:

When a sapphire disc was used as one of the contact surfaces, the shape and thickness of the anomalous films, and the traction coefficient were almost symmetrical with respect to the sign of the side-to-roll ratio. In contrast, when a glass disc was used, they were not symmetrical at a low ambient temperature. In the case of a glass disc, thicker films and smaller traction coefficients were observed at negative slide-to-roll ratios, whereas the film collapsed at positive side-to-roll ratios. The asymmetrical film shape approached a level of symmetry; this decreased the thickness of the film with increasing ambient temperature. The differences in the

trends of the film formation and traction behaviour with the changing material of one surface is attributable to the differences in the thermal properties between sapphire and glass. Sapphire has a relatively higher thermal conductivity than glass and comparable to that of steel; thus, it forms a symmetrical heat transfer field between the mating surfaces.

The phase state of the lubricant film was investigated using a simple temperature estimation model in comparison with the phase diagram of 1-dodecanol. When the phase of the lubricant film was in the solid state of the phase diagram, stable anomalous films were formed and were observed at the sapphire–steel contact. Conversely, when the film was in the liquid state of the phase diagram, some interesting phenomena were observed; the calculated temperature of the film was higher than the melting point resulting from the heat generation when the film collapsed at positive slide-to-roll ratios. When the ambient temperature increased, the film collapse behaviour was observed at negative as well as positive slide-to-roll ratios. The trend of the traction coefficient changed from that of a traction fluid to that of a viscous fluid with increasing ambient temperature; the traction coefficient increased monotonically with increasing slide-to-roll ratio. However, a small thickened part of the film remained around the central zone.

Acknowledgements This work was supported by JSPS KAKENHI Grant Number 21686016, Grant-in-Aid for Young Scientists (A). The authors express their gratitude to Dr T. Reddyhoff of Imperial College for providing them the equation of the transition line between the low and high friction phases of 1-dodecanol.

References

1. Bridgman, P.W.: Viscosities to 30,000 kg/cm². *Proc. Amer. Acad. Arts Sci.* **77**, 117–128 (1949)
2. Gohar, R., Cameron, A.: Optical measurement of oil film thickness under elastohydrodynamic lubrication. *Nature* **200**, 458–459 (1963)
3. Smith, F.W.: Lubricant behavior in concentrated contact systems—the castor oil–steel system. *Wear* **2**, 250–263 (1958)
4. Smith, F.W.: Lubricant behavior in concentrated contact—some rheological problems. *ASLE Trans.* **3**, 18–25 (1960)
5. Smith, F.W.: The effect of temperature in concentrated contact lubrication. *ASLE Trans.* **5**, 142–148 (1962)
6. Johnson, K.L., Tevaarwerk, J.L.: Shear behaviour of elastohydrodynamic oil films. *Proc. R. Soc. Lond. Ser. A* **356**, 215–236 (1977)
7. Evans, C.R., Johnson, K.L.: The rheological properties of elastohydrodynamic contacts. *Proc. Inst. Mech. Eng.* **200**, 303–312 (1986)
8. Evans, C.R., Johnson, K.L.: Regimes of traction in elastohydrodynamic lubrication. *Proc. Inst. Mech. Eng.* **200**, 313–324 (1986)
9. Grubin, A.N.: Investigation of the contact of machine components. In: Kh.F. Ketova (ed.) *Central Scientific Research Institute for Technology and Mechanical Engineers, Moscow (DSIR translation 337) vol. 30*, (1949).

10. Hamrock, B.J., Dowson, D.: *Ball Bearing Lubrication: The Elastohydrodynamics of Elliptical Contacts*. Wiley, New York (1981)
11. Venner, C.H., Lubrecht, A.A.: *Multi-level Methods in Lubrication*. Elsevier Science B.V, Amsterdam (2000)
12. Foord, C.A., Wedeven, L.D., Westlake, F.J., Cameron, A.: Optical elastohydrodynamics. *Proc. Inst. Mech. Engrs Part 1* **184**, 487–505 (1969–1970)
13. Nagaraj, H.S., Sanborn, D.M., Winer, W.O.: Surface temperature measurements in rolling and sliding EHD contacts. *ASLE Trans.* **22**, 277–285 (1979)
14. Wedeven, L.D.: Discussion to Najaraj's paper. *ASLE Trans.* **22**, 285 (1979)
15. Sanborn, D.M., Winer, W.O.: Fluid rheological effects in sliding elastohydrodynamic point contacts with transient loading: 1-film thickness. *Trans. ASME J. Lubr. Technol.* **93**, 262–271 (1971)
16. Sadeghi, F., Sui, P.C.: Thermal elastohydrodynamic lubrication of rolling/sliding contacts. *Trans. ASME J. Tribol.* **112**, 189–195 (1990)
17. Yagi, K., Kyogoku, K., Nakahara, T.: Temperature measurements of both sliding surfaces and estimation of temperature profile across film thickness under EHL conditions. *J. Jpn. Soc. Tribol.* **47**(4), 321–328 (2002)
18. Yagi, K., Kyogoku, K., Nakahara, T.: Experimental investigation of effects of slip ratio on elastohydrodynamic lubrication film related to temperature distribution in oil films. *Proc. Inst. Mech. Eng. Part J* **220**(4), 353–363 (2005)
19. Kaneta, M., Nishikawa, H., Kameishi, K., Sakai, T., Ohno, N.: Effects of elastic moduli of contact surfaces in elastohydrodynamic lubrication. *Trans. ASME J. Tribol.* **114**, 75–80 (1992)
20. Kaneta, M., Nishikawa, H., Kanada, T., Matsuda, K.: Abnormal phenomena appearing in EHL contacts. *Trans. ASME J. Tribol.* **118**, 886–892 (1996)
21. Yagi, K., Kyogoku, K., Nakahara, T.: Mechanism of dimple formation under elastohydrodynamic conditions. In: Dowson, D., Priest, M., Dalmaz, G., Lubrecht, A.A., (eds.) *Proceedings of the 29th Leeds-Lyon Symposium on Tribology*, Elsevier B. V., Amsterdam, pp. 111–120 (2003). [https://doi.org/10.1016/S0167-8922\(03\)80124-4](https://doi.org/10.1016/S0167-8922(03)80124-4)
22. Yagi, K., Kyogoku, K., Nakahara, T.: Relationship between temperature distribution in EHL film and dimple formation. *Trans. ASME J. Tribol.* **127**(3), 658–665 (2005)
23. Chiu, Y.P., Sibley, L.B.: Contact shape and non-Newtonian effects in elastohydrodynamic point contacts. *Lubr. Eng.* **28**, 48–60 (1972)
24. Yagi, K., Vergne, P.: Film thickness changes in EHD sliding contacts lubricated by a fatty alcohol. *Tribol. Online* **1**, 5–8 (2006)
25. Yagi, K., Vergne, P.: Abnormal film shapes in sliding elastohydrodynamic contacts lubricated by fatty alcohols. *Proc. Inst. Mech. Eng. Part J* **221**, 287–300 (2007)
26. Yagi, K., Sugimura, J., Vergne, P.: Rheological response of fatty alcohols in sliding elastohydrodynamic contacts. *Tribol. Int.* **49**(5), 58–66 (2012)
27. Wang, P., Reddyhoff, T.: Wall slip in an EHL contact lubricated with 1-dodecanol. *Tribol. Int.* **113**, 197–205 (2017)
28. Yagi, K., Nishida, K., Sugimura, J.: Relationship between molecular structure of lubricant and appearance of anomalous film shapes in elastohydrodynamic lubrication conditions. *Tribol. Int.* **152**, 106574 (2020)
29. Yagi, K., Nishida, K., Sugimura, J.: Traction behaviour of elastohydrodynamic lubrication films with anomalous shapes. *Proc. Inst. Mech. Eng. Part J.* **221**, 287–300 (2017)
30. Reddyhoff, T., Ewen, J.P., Deshpande, P., Frogley, M.D., Welch, M.D., Montgomery, W.: Macroscale superlubricity and polymorphism of long-chain *n*-alcohols. *ACS Appl. Mater. Interfaces* **13**, 9239–9251 (2021)
31. Cameron, A.: The viscosity wedge. *ASLE Trans.* **1**, 248–253 (1958)
32. Piermarini, G.J., Block, S., Barnett, J.D., Forman, R.A.: Calibration of the pressure dependence of the R1 ruby fluorescence line to 195 kbar. *J. Appl. Phys.* **46**, 2774–2780 (1975)
33. Reddyhoff, T., Schmidt, A.S., Spikes, H.: Thermal conductivity and flash temperature. *Tribol. Lett.* **67**, 22 (2019)
34. Habchi, W., Bair, S.: The role of the thermal conductivity of steel in quantitative elastohydrodynamic friction. *Tribol. Int.* **142**, 105970 (2020)
35. Liu, H.C., Zhang, B.B., Bader, N., Poll, G., Venner, C.H.: Influences of solid and lubricant thermal conductivity on traction in an EHL circular contact. *Tribol. Int.* **146**, 106059 (2020)
36. Carareto, N.D.D., Costa, M.C., Meirelles, J.A.A., Pauly, J.: High pressure solid–liquid equilibrium of fatty alcohols binary systems from 1-dodecanol, 1-tetradecanol, 1-hexadecanol, and 1-octadecanol. *J. Chem. Eng. Data* **60**(10), 2966–2973 (2015)
37. Bridgman, P.W.: Effects of high shearing stress combined with high hydrostatic pressure. *Phys. Rev.* **48**, 825–847 (1935)
38. Sasaki, K., Inayoshi, N., Tashiro, K.: In situ FTIR-ATR observation of phase transition behavior of *n*-alkane molecules induced by friction motion on a metal interface. *J. Phys. Chem. C* **113**, 3287–3291 (2009)
39. Cann, P.M., Spikes, H.A.: In-contact IR spectroscopy of hydrocarbon lubricants. *Tribol. Lett.* **19**(4), 289–297 (2005)
40. Findenegg, G.H.: Order-disorder transitions at the liquid/solid interface. Volumetric behaviour of primary aliphatic alcohols near the graphon surface. *J. Chem. Soc. Faraday Trans.* **1**(68), 1799–1806 (1972)
41. Findenegg, G.H.: Ordered layers of aliphatic alcohols and carboxylic acids at the pure liquid/graphite interface. *J. Chem. Soc. Faraday Trans* **1**(69), 1069–1078 (1973)
42. Bien-Vogelsang, U., Findenegg, G.H.: Monolayer phase transitions of dodecanol at the liquid/graphite interface. *Colloids Surf.* **21**, 469–481 (1986)
43. Yeo, Y.H., McGonigal, G.C., Thomson, D.J.: Structural phase transition of a 1-dodecanol monolayer physisorbed at the liquid/graphite interface by scanning tunneling microscopy. *Langmuir* **9**(3), 649–651 (1993)
44. Castro, M.A., Clarke, S.M., Inaba, A., Thomas, R.K.: Solid monolayers adsorbed at the solid–liquid interface studied by incoherent elastic neutron scattering. *J. Phys. Chem. B* **101**(44), 8878–8882 (1997)
45. Ocko, B., Hlaing, H., Jepsen, P., Kewalramani, S., Tkachenko, A., Pontoni, D., Reichert, H., Deutsch, M.: Unifying interfacial self-assembly and surface freezing. *Phys. Rev. Lett.* **106**, 13801 (2011)

Publisher's Note Springer Nature remains neutral with regard to jurisdictional claims in published maps and institutional affiliations.